Title

The Development of High Energy Storage Capacity Li-ion Battery Anode Material and Quantitative Analysis of Solid Electrolyte Interphase

Author

Zhang, Xinyue

Publication Date

2023

Peer reviewed|Thesis/dissertation

UNIVERSITY OF CALIFORNIA

Los Angeles

The Development of High Energy Storage Capacity Li-ion Battery Anode Material and Quantitative Analysis of Solid Electrolyte Interphase

A thesis submitted in partial satisfaction

of the requirements for the degree Master of Science

in Chemical Engineering

by

Xinyue Zhang

2023

ABSTRACT OF THE THESIS

The Development of High Energy Storage Capacity Li-ion Battery Anode Material and Quantitative Analysis of Solid Electrolyte Interphase

by

Xinyue Zhang

Master of Science in Chemical Engineering

University of California, Los Angeles, 2023

Professor Yuzhang Li, Chair

In the domain of modern lithium-ion batteries, the anode material plays a critical role in ensuring safe and reliable storage of the battery's capacity for efficient rechargeability. However, the commercial graphite material currently utilized is constrained by its limited volumetric and gravimetric capacity, as well as its proximity to Li plating hazards. With the growing demand for increased energy storage capacity and power density, there is a significant focus on exploring new electrode materials that offer higher specific and areal capacity, scalable synthesis methods, faster charging capabilities, improved safety standards, stable cycling performance, and lower cost. Also, with the development of microscopic techniques, the knowledge gap between battery performance

and microscopic changings in cell configuration, such as solid-electrolyte interphase, can be further investigated. This works aims to explore the relevant criteria through the examination of surface modified (graphitic carbon coated) silicon as a potential anode material and the investigation of a multifunctional solid electrolyte interface (SEI) as a solid-state electrolyte. The primary objective is to advance the understanding of these key components and their interactions, ultimately driving innovation in the field of high-performance batteries. Throughout this thesis, the cyclability of bare Si anode is improved and the electrochemical properties of SEI can be quantitatively measured and correlated to battery performance.

The thesis of Xinyue Zhang is approved.

Richard B. Kaner

Carlos Gilberto Morales Guio

Yuzhang Li, Committee Chair

University of California, Los Angeles

2023

Table of Content

List of Figures

Acknowledgement

This work is the result of collective contributions from numerous individuals. I would like to express my gratitude to the external scientific collaborators, peers, and mentors who have made valuable contributions to my projects in various capacities (Spencer Hamilton, Xueying Chang, Cheng-Wei Lin from the Kaner Lab, Jinhui Xu and Qingyang Yin from the Lu Lab) and my lab mates from the Li Group (among many others, Bo Liu, Grace Vasiknanonte, Xintong Yuan). Their support and insights have been instrumental in shaping the outcomes of this work, and I am sincerely thankful for their contributions. I would like to express my deepest gratitude to my advisor, Professor Yuzhang Li, for providing me with the invaluable opportunity to explore and grow as a graduate researcher throughout my journey in various research topics. His inspiration and mentorship have been instrumental in my academic and personal development.

I would like to give special thanks to Professor Richard Kaner and Professor Carlos Morales-Guio for being my thesis committee and reviewing this work. I extend my heartfelt appreciation for the patience and time dedicated by everyone involved in this work. I am also grateful for the teaching opportunities provided by Professor Johnny Pang in the Chemistry Department, which not only offered me valuable teaching experience but also served as a source of financial support during my master's studies.

At the end, I would like to thank my parents and family for financially and spiritually supporting me through my international study period. Also, I want to thank my special one, Gan Yang, for his positive companionship and constant encouragement throughout the years.

Introduction

The issue of global carbon growth has emerged as a critical concern in the fight against climate change. Up until 2022, the International Energy Agency (IEA) has reported that the global energy-related carbon growth has reached the historical climax of about 36.8 Gt with a growth rate of 321 Mt per year.[1] Despite the notable slowdown in the growth rate of global carbon emissions in recent years, attributed in part to the unprecedented disruption caused by the COVID-19 pandemic, efforts toward sustainable technology development have remained relentless. Within the past year, the remarkable expansion of solar photovoltaic (PV) and wind power generation has played a pivotal role in mitigating approximately 465 million metric tons (Mt) of carbon dioxide (CO_2) emissions in the power sector; the combined efforts of other renewable energy sources, electric vehicles (EVs), and heat pumps have prevented an additional approximate 85 Mt.[2,3] A recent report by McKinsey & Company, a leading global consulting firm, provides valuable insights into the trajectory of carbon emissions and the urgent need.[2,4] Among the various endeavors dedicated to combating climate change, battery development plays a crucial role in enabling the integration of renewable energy into existing grids and enhancing energy storage capabilities. By efficiently storing energy generated from sources such as solar and wind power, batteries overcome the intermittent nature of renewable energy, ensuring a reliable and consistent power supply. This synergy between battery technology and decarbonization allows for a cleaner and more sustainable energy ecosystem.

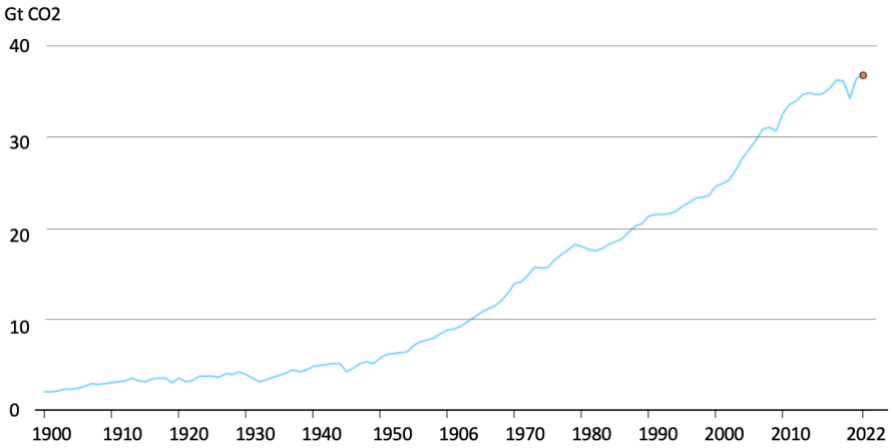

Figure 1. Global CO_2 Emission from Energy Combustion and Industrial Processes [1]

One of the most prominent and widely used battery technologies is lithium-ion (Li-ion) batteries. Li-ion batteries have revolutionized the energy landscape with their high energy density, longer lifespan, and rapid charging capabilities. They have found applications in various sectors, including electric vehicles (EVs), renewable energy storage systems, and portable electronics. According to a recent McKinsey & Company report, the global demand for Li-ion batteries is expected to soar over the next decade, with the number of GWh required increasing from about 700 GWh in 2022 to around 4.7 TWh by 2030 (Figure 2). Batteries for mobility applications, such as electric vehicles (EVs), will account for the vast bulk of demand in 2030—about 4,300 GWh[4]; an unsurprising trend seeing that mobility is growing rapidly.

Figure 2. Global Li-Ion Battery Cell Demand [2]

A conventional battery is an ensemble of multiple electrochemical components including cathode, anode, electrolyte, current collector, separator, and conductive cases. In recent years, graphite has been commonly used as the commercial anode material, while NMC and LFP compounds serve as the cathode materials.[5,6] However, with the growing demand for increased energy storage capacity and power density, there is a significant focus on exploring new electrode materials that offer higher specific and areal capacity, scalable synthesis methods, faster charging capabilities, improved safety standards, stable cycling performance, and lower cost. Furthermore, the investigation of solid-state electrolytes has gained considerable attention among research groups. Solid-state electrolytes have emerged as a promising alternative to traditional organic liquid electrolytes since they can effectively eliminate the safety concern of flammability and leakage, exhibiting higher chemical, electrochemical, thermal, and mechanical stability over long cycles.

This thesis report primarily focuses on two research projects: the examination of surface-modified (graphitic carbon coated) silicon as a potential anode material and the investigation of a multifunctional solid electrolyte interface (SEI) as a solid-state electrolyte. The primary objective is to contribute to the development of battery technology with high energy storage capacity and

easily synthesized electrode material as well as to bridge the knowledge gap between existing electrolyte chemistry and its impact on SEI properties and battery performance. The aim is to advance the understanding of these key components and their interactions, ultimately driving innovation in the field of high-performance batteries.

Silicon Anode

Background

With the increasing demand on high energy density storage material, the investigation of potential electrode materials in the field of rechargeable Lithium Ion Batteries has attracted people's attention over the past decades. Many of the reported electrode materials have been found and evaluated from the perspective of specific capacity, specific energy, cyclability, durability, ionic diffusivity, and conductivity, etc. With the benefit of superior theoretical capacity (4200 mAh/g, $Li_{4.4}Si$)[7], silicon, a cheap, non-toxic, and abundant material, is highlighted as a promising anode material in lithium-ion batteries (LIBs). Besides, the moderate lithiation potential of Si vs. Li/Li^+ (~0.4 V), it can effectively avoid the problems caused by Li deposition in graphite anodes (~0.2 V vs. Li/Li^+) and leads to only a minor energy penalty compared with other metal oxides anode materials (>1 V vs. Li/Li^+).[8] In addition, the abundance of elemental silicon in the earth's crust mitigates the gap between economic efficiency and industrial application. However, the practical silicon application in LIBs is still severely hindered by three main problems: the huge volume expansion (>300%) due to the phase transformation of Li-Si alloy during charging and discharging cycles,[7] the continuous growth of the solid electrolyte interface, and the low intrinsic electronic conductivity of Si. In practice, the volume expansion of silicon can cause mechanical failure of the electrode and loss of conductive pathways; the continuous growth of SEI on the freshly exposed surface will irreversibly consume the lithium resource within the system and lead to short cyclability, irreversible capacity drop, and low coulombic efficiency; also as a promising electrode material, it is mandatory to sustain a certain level of electrical and ionic conductivity to efficiently transfer the electrons and ions during the charging and discharging processes. Although

tremendous efforts have been made to address these issues, such as nanostructure engineering, multifunctional polymer binder, surface engineering, novel electrolyte additives, and hybrid composites,[7,9–16] the adoption of silicon micro size particles (SiMPs) has not yet been leveraged to its full extent to embrace all the challenges simultaneously. **In this project, we believe it would be more meaningful to tackle the challenges of micro-size silicon as the areal capacity is significantly larger than nano particles and the production cost is much lower than nano engineering**.

Hypothesis

In this project, we aim to enhance the performance of silicon anodes in LIBs by overcoming one of the barriers mentioned in the previous section. The ultimate goal is to form a conformal graphitic carbon coating on micro-size silicon via either the Pickering Emulsion Method or the High Energy Arc Welding method so that we can constraint the volume expansion of silicon with mechanical support and improve the electrical conductivity of pristine silicon.

Methodology and Experimental Set-up

a) Pickering Emulsion

The method of Pickering Emulsion is inspired by the application of conformal graphene coating on Ni-rich LiNi0.8Co0.15Al0.05O2 (NCA) cathode powder.[17] A Pickering Emulsion requires two immiscible solvents with appropriate solvent-exfoliated interphase surfactant that can stabilize at the boundary of emulsion droplets over time.[18] With the benefit of simplicity and mass production, it has been applied to in-situ polymerization and thin-layer conformal coating.[17,19]

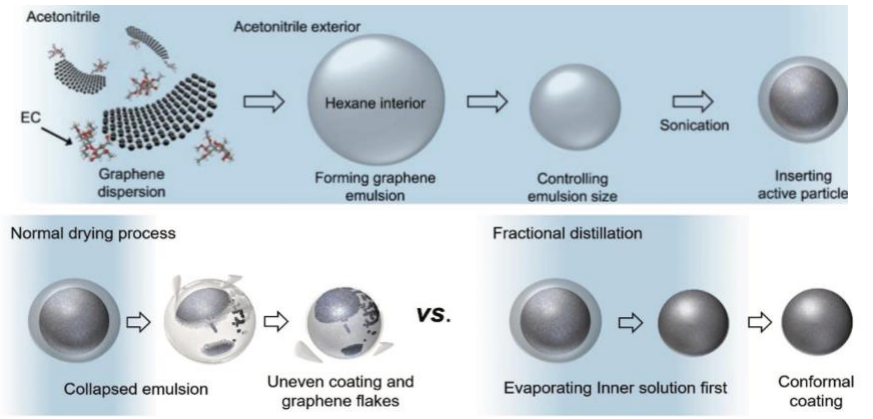

Figure 3. Schematic of Pickering Emulsion of Ni-rich NCA Cathode Powder [17]

Choice of Material:

The potential solid interphase surfactant/coating material in the Pickering Emulsion method is graphene and graphite oxide (which can be reduced to graphene through laser scribing) since both can provide fair mechanical support and sufficient electrical conductivity to overcome the obstacles of silicon volume expansion, poor conductivity, and loss of conductive pathways during battery cycling. Also, the choice of potential solvents must satisfy a few requirements: first, the two immiscible solvents must have distinct boiling points so that eventually the interior and exterior solvent can evaporate distinctively in order during the fractional distillation process (Figure 3. Schematic of Pickering Emulsion of Ni-rich NCA Cathode Powder); second, the interior emulsion droplets must have better selectivity to the active particles (Si) compared with the exterior solvent; third, the interior emulsion droplets must have attractions to graphene (Gr)/graphite oxide (GO), so that the surfactant can stabilize at the solvent interphase over time under light fluctuation; and last but not least, the solvent system must have good uniform dispersion of Gr/GO to form a conformal coating outside the active particles. In this experiment, we tried different solvent combinations including water, ethanol THF, acetonitrile, hexane, toluene,

acetone, aniline, octane, and 1-octadecene. (All of the solvents have a reasonable boiling point within the range of our laboratory evaporation technique.)

Among all the solvent combinations, the optimized final setup utilizes 1-octadecene and water as the exterior and interior solvents. The emulsion system has the best stability over time (24 h) and the boiling point of water and 1-octadecence are 100 °C and 315 °C, respectively. According to our experimental results, silicon with a native oxide layer (~20 nm thickness[20]) favors the water droplets and repels the oil solvent, so that the active material can be encapsulated well inside the water emulsion droplets. In addition, we choose graphene with 7% nitrogen additive as the solid surfactant since it can disperse uniformly in 1-octadecene and the polar tail favors the stabilization at the surface of the water droplets.

Experimental Setup and Procedure

Preparation of Pickering Emulsion

The initial step of the Pickering Emulsion coating method is to disperse the solid surfactant (Graphene 7%N) uniformly into the organic solvent, 1-octadecene (5 mL). Here, we add some ethyl cellulose (Gr:EC = 1:2) and/or F-127 (0.3 wt%) to assist the uniformity of dispersion. With approximately 2 hours probe sonication at 70% power amplitude, the surfactant can stabilize inside the organic solvent over 2 h at room temperature. Then, we add the interior solvent (water) at a volume ratio of 1/5 of the exterior solvent, along with 1 min of vortexing to generate an even emulsion mixture. This ratio of solvent is optimized based on our observation under the optical microscope. If the ratio of the interior solvent is increased in the emulsion, it will result in an increase in the size of the emulsion droplets. Similarly, decreasing the ratio of the interior solvent will also lead to a larger droplet size in the emulsion. Considering that the active material (SiMP)

is approximately 1-3 μm, it would be desirable to have control over the emulsion droplet size. Specifically, the droplet size should be large enough to encapsulate the active particles, but small enough to ensure that there is only one particle per droplet.

According to previous research, the ratio of surfactant and active material (Si) must be at least 5 wt% to achieve a conformal coating on the surface. Also, the standard recipe of Silicon anode slurry includes 5~10 wt% conductive material (such as carbon black or super P). In this experiment, we first add 1.375 mg of graphene (7%N) into 5 mL of organic solvent and 1 mL of water as mentioned; then we add 275 mg of Silicon into the pre-made emulsion mixture (Graphene-Octadecene-Water).

Fractional Distillation

To obtain the graphene coated SiMPs, we use the fractional drying procedure (Figure 3) to evaporate the solvent system. The equipment we used included a rotatory evaporator and a heating mantle distillation setup. The liquid mixture with silicon coated inside the emulsion droplets subsequently undergoes a fraction distillation using a rotatory evaporator, where the interior droplets are removed first, and the exterior solvent is removed afterward. Eventually, an additional calcination step at 600 °C for 1 h can carbonize the dispersants (i.e., ethyl cellulose or F-127) used during the process.

Figure 4. Experimental Set-up for Pickering Emulsion of SiMPs: Rotatory Evaporator (Left); Distillation Kit (Right)

Slurry Fabrication

The collected carbon coated silicon (Si@C) is tested in coin cells using conventional slurry method. The active material (Si@C) is mixed with an aqueous-based binder material, carboxymethyl cellulose (CMC), and a conductive additive, carbon black, in a mortar and pestle in a mass ratio of 8:1:1. After evenly distribute the powder, DI water is added as the solvent to achieve a uniform and spreadable slurry. Then, the resulting slurry is casted onto a Cu foil with a thickness of 8 μm and dried in a vacuum oven overnight (for at least 8 hours) at 90 °C. The dried electrode slurry is pressed at 3 metric tons using hydraulic press for 5 min and punched into circular discs of 12 mm diameter size with a mass loading of 0.5-0.8 mg/cm^2

b) PDA Coating and High Energy Arc Welding

In parallel to the Pickering Emulsion method, dopamine is another potential carbon source of coating with relatively low cost and ease of fabrication. It has the ability to undergo self-

polymerization and deposit conformal polydopamine (PDA) films spontaneously on nearly any surface under basic conditions.[21] Under high-temperature joule heating conditions, the PDA coating layer may transform into graphitic carbon, which can provide high conductivity and solid mechanical support for the Silicon anode material. The method of high-energy joule heating in this part of the project is determined between Laser Scribe, Arc Welding, and High-Temperature Furnace.[22] The highlight of flash joule heating and micro-size silicon differentiate this project from the previous work of PDA coating on SiNPs.[21] The ultimate goal of this part is to enhance the electrochemical performance of micro-size silicon anode efficiently through practical and cost-effective methods.

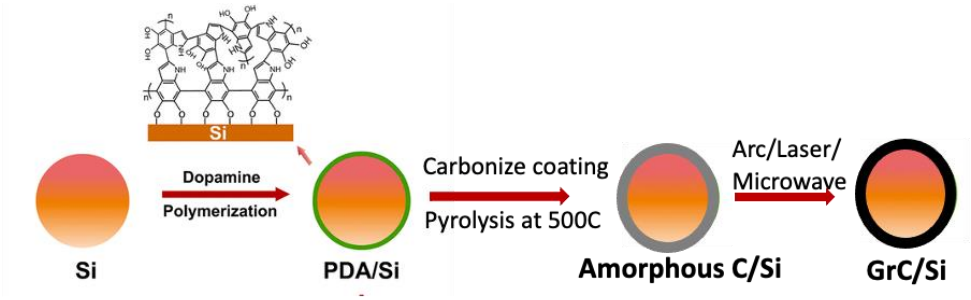

Figure 5. Schematic of PDA Polymerization[21] and Graphitization of Carbon Shell via Pyrolysis and Arc Welding

Experimental Setup and Procedure

Preparation of PDA coated-SiMPs

The synthesis process for producing PDA coated SiMPs is inspired by the pioneering work on the application of PDA on graphite oxide/silicon composite.[21] The schematic protocol is illustrated in Figure 5. Initially, SiMPs are uniformly dispersed in a mixture of 95% ethanol and water mixture (4:3 vol ratio) together with the PDA precursor, Dopamine Hydrochloride (Sigma Aldrich), through bath sonification. Then, the formation of PDA coating proceeds with the addition of 1 M,

pH = 8.5 Tris-HCl Buffer solution (BBP). Due to the robust and irreversible binding between Si-OH on the surface of native silicon oxide in an aqueous solution and the catechol-functional group in polydopamine, a conformal coating of the PDA layer can form at room temperature through polymerization. During the polymerization process, it is clear to observe that SiMPs change color significantly from pale grey to dark black. According to our experimental data, the concentration of buffer solution and the volume ratio will adversely affect the thickness of the PDA layer and the mass ratio of PDA precursor to silicon (1:1wt%) would yield 10% carbon coating after the carbonization step.

High Energy Arc Welding

Arc Welding is a commonly applied engineering process that transforms electrical energy into thermal energy. It can create intense heat up of around 6500 F by passing an electric current through an electrode, which is typically made of a metal or alloy that is compatible with the base material being welded.[23] In order to have a uniform welding product, it is essential to have a conductive material prior to the arc welding step, so that the electricity can be evenly distributed over the surface of the target material. This experiment was conducted through a homemade Arc Welding set-up under Ar environment (Figure 6).

Figure 6. Experimental Set-up for Arc Welding: Hydraulic Press (left) and Home-made Arc Machine (right)

To improve the conductivity of active material before arc welding, the PDA coated silicon must be carbonized first through a short pyrolysis step at 300 C, which can convert the polymer layer to amorphous carbon while enhancing the conductivity of the material. The product obtained from the polymerization step through vacuum filtration is initially furnaced under a Nitrogen environment for 1 hour. Then, the pyrolyzed carbon coated Si (Si@C) is arc welded in the form of a pellet (pressed at 3 metric ton force) under different power and time conditions. The goal is to find the optimized Arc power with a minimum amount of time to convert the amorphous carbon layer to graphitic carbon (at around 3140 F) without forming silicon carbide (side product).[24–26] Eventually, the final product is ground into powder by mortar pestle for XRD, Raman, and electrochemical performance analysis (in slurry electrode coin cells) in the result section.

Result and Discussion

a) Pickering Emulsion

Preliminary Result

From the experimental observation, initially, the graphene is evenly dispersed in the organic solvent, 1-octadecene, on the top layer before vortexing. After vortexing for a minute, the black layer "precipitates" to the bottom since we expect that most of the graphene should stabilize at the surface of water droplets, which are heavier than the organic solvent. Moreover, we confirm that most of the graphene stabilizes at the droplet interphase through the optical microscopic images. Eventually, with the addition of SiMPs, the majority of SiMPs favor staying inside the water droplets (Figure 8).

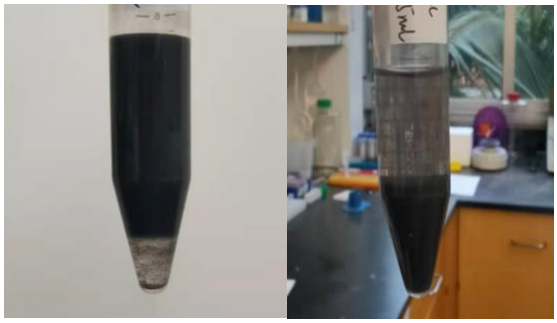

Figure 7. Formation of Pickering Emulsion via Vortex: Before Vortex (left) and After Vortex (right)

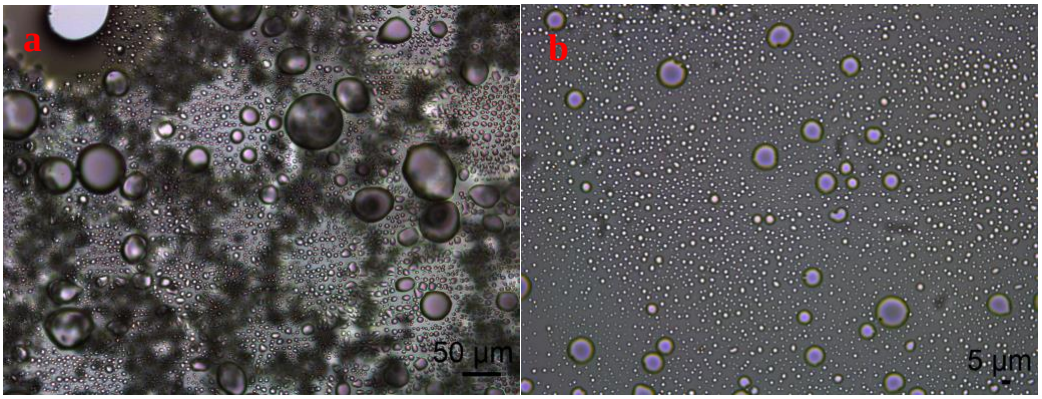

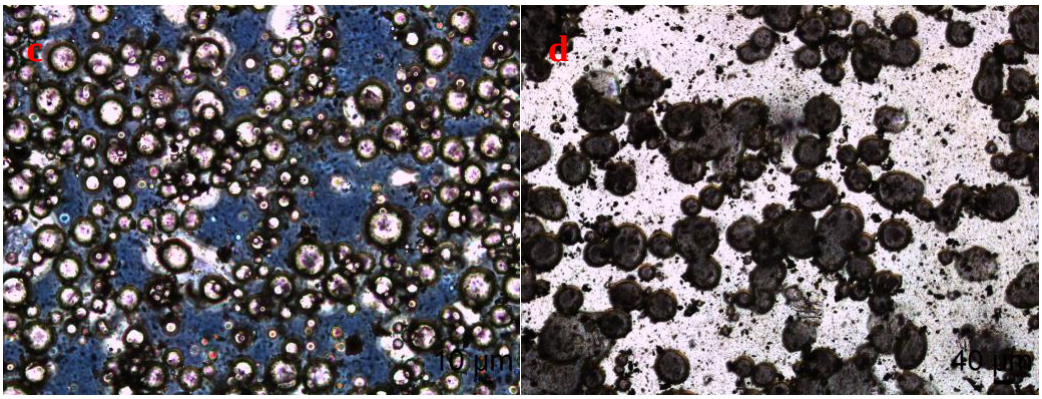

Figure 8. Graphene Pickering Emulsion Based on Water and 1-Octadecene: Size change of emulsion droplet with changing water to Octadecene volume ratio a) 1:3 w/o; b) 1:5 w/o; c) Magnified optical microscopy of graphene Pickering Emulsion; d) Magnified optical microscopy of encapsulated SiMPs

Besides the optical microscopic results, we also performed transmission electron microscopy (TEM) analysis. According to the TEM image of the final product of the Pickering Emulsion, most of the SiMPs are wrapped inside/in between the graphene sheets.

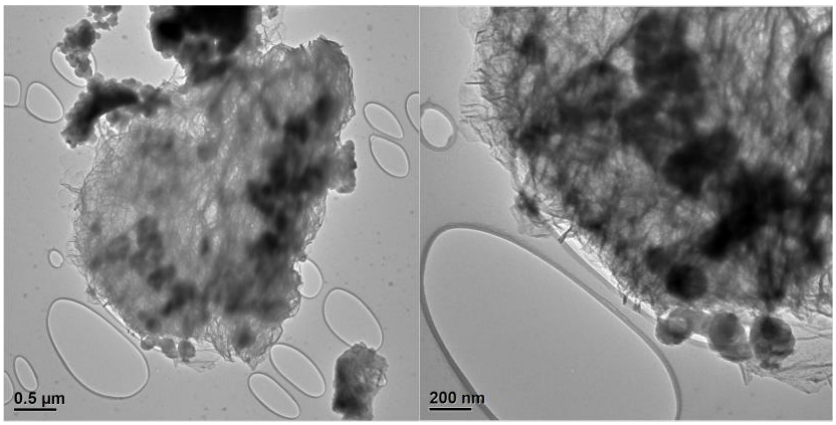

Figure 9. Graphene encapsulated silicon particles

Then, the graphene coated silicon product obtained through fractional distillation is collected to make electrode slurry (details in method section). As another optical evidence, the color of coated material (Figure 10 top) is significantly darker than pristine silicon (Figure 10 bottom). This further confirms that with 5% graphene (7%N), most of the silicon particles are coated evenly through the Pickering Emulsion step.

Figure 10. Electrode Slurry of Graphene coated Si on Cu Substrate: Graphene (7%N) coated Silicon (Up) and Bare Silicon (1-3 μm) (bottom)

According to the preliminary experimental result, the best solvents fulfilling all the requirements simultaneously are water and 1-octadecene (1:5) among all the liquid solvents (water, ethanol, acetonitrile, hexane, octane, octadecene, THF, toluene, and aniline). The solid surfactant is chosen to be graphene with 7% nitrogen additive (Gr+7%N) after comparing with GO, graphene, and alkylated GO. Preliminary electrochemical data illustrates that the SiMP-Gr material after the Pickering Emulsion can enhance the capacity retention (24.8% after 10 cycles) compared with pristine SiMP (6.8% after 3 cycles) charging at C/20. The usage of dual salt electrolyte (0.6MLiDFOB+0.6MLiBF$_6$) together with the Pickering emulsion SiMP-Gr can further increase the capacity retention to 36.7% after 20 cycles (Figure 3a). In addition, the initial Coulombic Efficiency is improved from 70.57% (pristine SiMPs) to 81.96% (SiMP-Gr). With the addition of dual salt electrolyte, the Coulombic Efficiency can stabilize over 99% after activation cycles (Figure 11b).

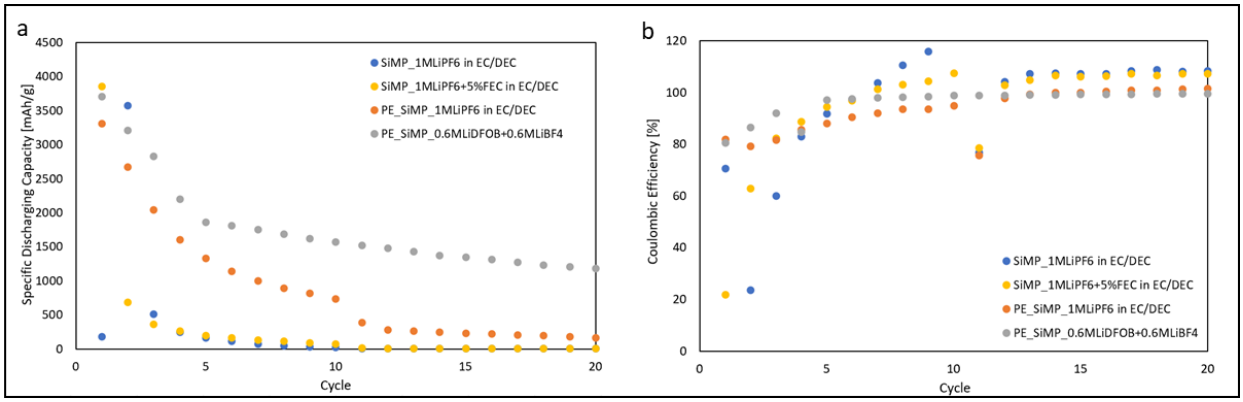

Figure 11. Electrochemical performance of Silicon Anode with Graphene coating after Pickering Emulsion.

Discussion

According to the electrochemical performance and SEM images (Figure 9), graphene coating through the Pickering Emulsion method does not provide strong mechanical support or cannot achieve uniform conformal coating over the micro-size silicon particles. This may be due to several reasons: first, SiMPs can easily leak through the interior emulsion droplets due to their heavy mass and large volume. Hence, it is harder to avoid or eliminate the portion of uncoated Si. Second, the Van der Waals forces between graphene and SiMPs as well as the soft graphene sheet structure is not strong enough to constrain the mechanical force caused by volume expansion. SiMPs can only adhere to (or be wrapped by) the 2D graphene sheet after Pickering Emulsion, therefore, the "coating" mainly improved the electronic conductivity instead of mechanical support.

b) PDA Coating and High Energy Arc Welding

Preliminary Result

Initially, the method of PDA coating on the SiMPs surface is optimized under different synthesis conditions. It is observed that the uniformity of PDA coating can change with changing

concentration of ethanol and PDA precursor to SiMPs ratio. The ultimate goal is to use a minimum amount of PDA precursor to achieve a conformal coating since the PDA will eventually become graphitic carbon under pyrolysis and arc welding process, while carbon has ten times less capacity than silicon as anode active material. According to the SEM images of PDA coated SiMPs in Figure, it will be sufficient to obtain a fairly uniform coating with a 1.5 mass ratio of PDA precursor: SiMPs and 40 ml Ethanol/30 ml water solvent system (as ethanol will slow down the polymerization process, which may improve the uniformity of coating).

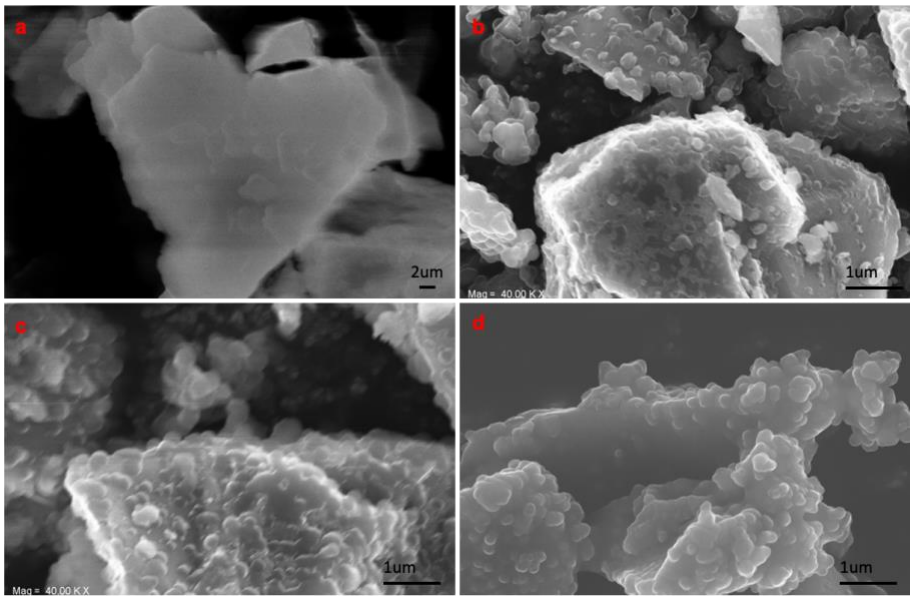

Figure 12. Morphology of PDA coated Silicon with changing mass ratio of PDA precursor to Si and ethanol concentration: a) Pristine Silicon Particle; b) 1:1 PDA precursor to Si; c) 1.5:1 PDA precursor to Si; d) 1.5:1 PDA precursor to Si with ½ ethanol concentration.

Then, the PDA coated products are pyrolyzed under 300 °C for 1 hour to carbonize the polymer layer as well as improve the conductivity of the product. As previously mentioned, it is mandatory to have great electrical conductivity before the process of arc welding, since the concept of arc welding transforms electrical energy into thermal heat. The conductive coating surface is required to conduct a uniform arc.

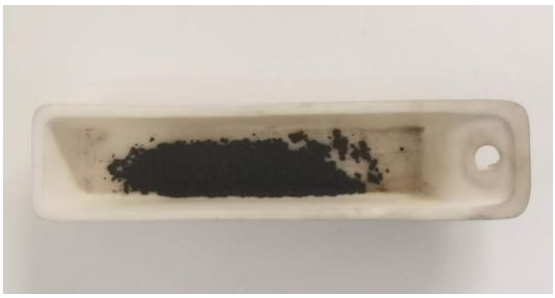

Figure 13. Optical Image of PDA coated Si after pyrolysis

After pyrolysis, the product is pressed with a hydraulic press under 3 metric tons force to prevent any powder splash caused by the arc tip. In this project, we test different arc conditions over different time scales to achieve the best coating with a minimum formation of by-products. It is noticed that the major by-product in this experiment is silicon carbide, which has strong mechanical properties as well as a slow side reaction rate but low specific capacity as battery materials (960 mAh/g).[27] Also, it is easy to sinter the PDA coated silicon with high energy Arc welding and long exposure time. According to the XRD analysis of the arced samples, the samples that undergo 30% arc power with 10-15 s exposure time show less amount of SiC by-product compared with the samples arced by 50% power and 75% power for 3-5 s. Since further decreasing the arc time will lead to non-uniform welding, we finalize the arc condition as 30% arc power and 10-15 s exposure time.

Figure 14. Arc Welded PDA coated Si Pellet via various power and time conditions: 1)75% power 3s; 2) 50% power 5s; 3) 50% power 3s; 4) 30% power 10s; 5) 75% power 3s; 6) 30% power 15s.

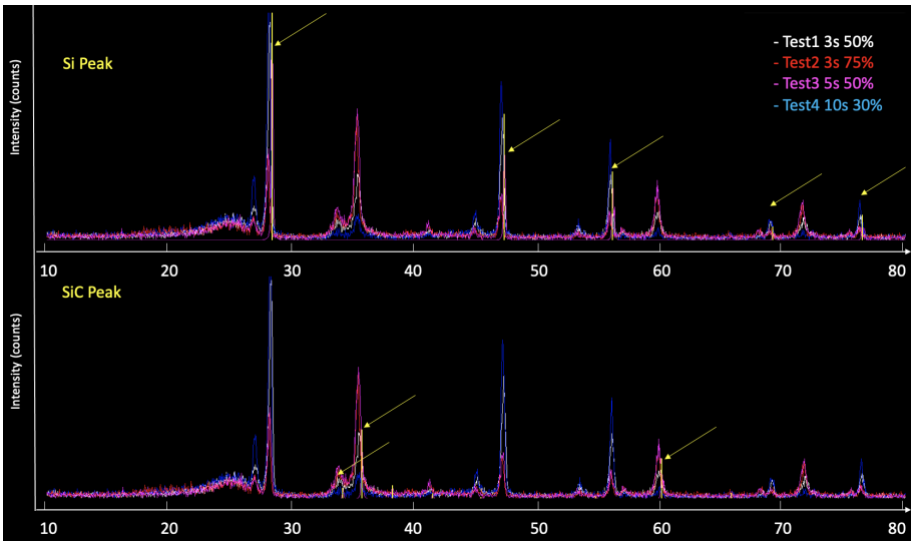

Figure 15. XRD spectrum of Arced PDA coated Si

Besides XRD analysis, we also conduct Raman tests to evaluate the quality of the graphitic carbon shell. In the Raman spectrum of carbon-based materials, a D band (at 1340 cm^{-1}) is ascribed to the disorder induced mode, while a relatively sharp peak at 1575 cm^{-1}, also named as G band, is ascribed as the E2g mode related to the sp2 carbon. To evaluate the degree of crystallization as well as the quality of graphitic carbon, the relative ratio of D band and G band (I_D/I_G) in the Raman spectra is a commonly used parameter to assess the structural disorder or defects in carbon-based

materials, such as graphene or carbon nanotubes. In general, a higher I_D/I_G ratio indicates a higher amount of structural disorder or defects, while a lower ratio suggests a more ordered and pristine structure. In our experimental results, it is assumed that the amorphous carbon layer outside silicon particles after pyrolysis will have a higher I_D/I_G ratio than the arc welded samples as amorphous carbon can transform into graphitic carbon under high-temperature annealing process at about 2000 degree Celsius under inert or reducing environment. This step is also referring as the graphitization process in which the rearrangement of carbon atoms from a disordered or amorphous state transforms into a more ordered and crystalline structure resembling graphite. As summarized in Table, the I_D/I_G ratio indeed decreases with increasing arc power and time of exposure. It seems that the optimum arc condition with a minimum amount of SiC by-product and lowest I_D/I_G ratio (minimun structural disorders and defects) is 30% power over 15 s.

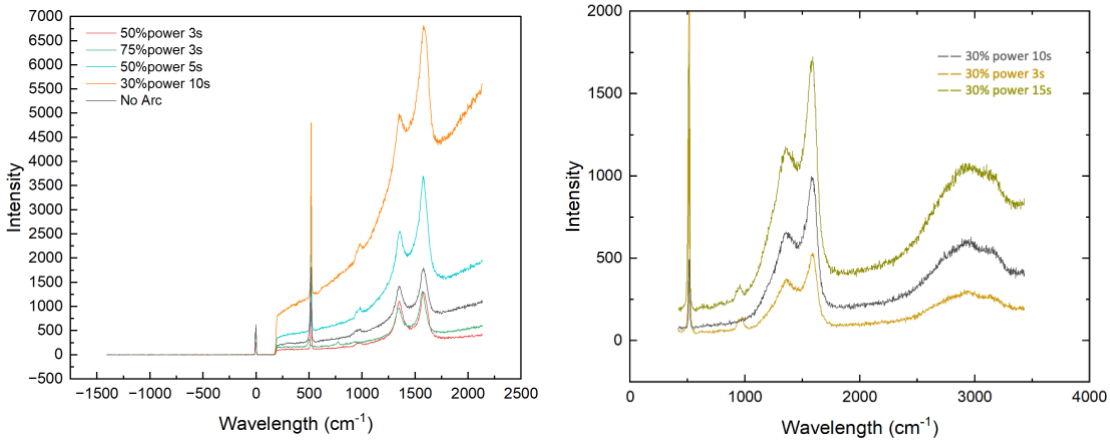

Figure 16. Raman Spectroscopy of Arced PDA coated SiMPs

Table 1. Summary of the relative ratio of D band/ G band over different arc conditions

Arc Power	Exposure Time (s)	I_D/I_G
0%	0	0.81
30%	10	0.74

30%	15	0.68
50%	3	0.85
50%	5	0.68
75%	3	0.79

Furthermore, the electrochemical tests are conducted to examine the cycling performance and specific capacity of the coated silicon anode material. It is observed that the initial specific capacity of PDA coated silicon after arc welding decreases compared with bare silicon material. This is due to the existing side-product SiC and carbon layers inside the anode mixture. Without carbon coating, pristine SiMPs will lose capacity after 3 cycles (6.8% capacity retention) due to pulverization. While PDA coating and arc welding enhance the capacity retention to about 400mAh/g after 20 cycles (which was 20% of the initial specific capacity). In addition, the initial Coulombic Efficiency is improved from 23% (pristine SiMPs) to 63% (PDA coated 30% arc 15 s) and the average Coulombic Efficiency is above 92% over the first 20 cycles. Although the performance is not comparable to pristine SiMPs with dual salt electrolyte, it shows some improvement compared with pristine silicon.

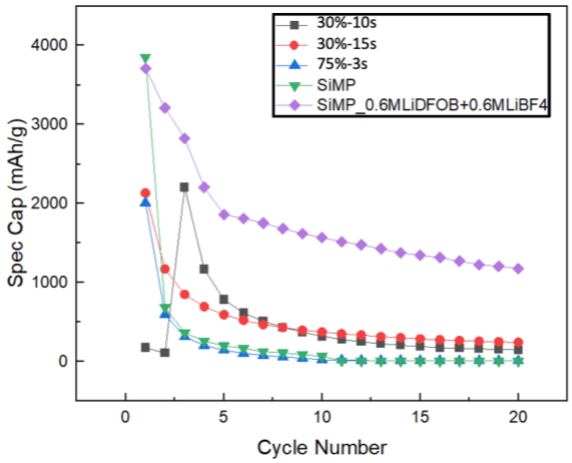

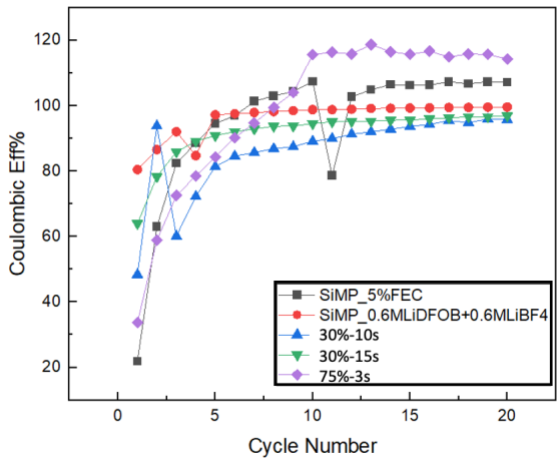

Figure 17. Electrochemical Performance of Arced PDA coated SiMPs

Discussion

According to the electrochemical performance, the specific capacity of the arced PDA coated Si (400 mAh/g) is very similar to graphite material (372 mAh/g). The improvement of Coulombic Efficiency is not even as significant as using the dual salt electrolyte. This may be due to several reasons: first, the uniformity of graphitization through arc welding is hard to control. The homemade arc welding machine is hard to control digitally, especially over a few seconds, it does not have a digital power control. Hence, it is easy to over weld the material so that the majority part of the sample is either sintered or not well graphitized. Second, the shape of the bulk pristine silicon particles is very random under SEM images, this will increase the difficulties of uniform coating through the synthesis process. In addition, according to our experimental result, 80 mg SiMPs and 80 mg PDA precursor will yield 80.02 mg of carbon coated SiMPs after pyrolysis. Considering the weight loss during the filtration and transfer step, the thickness of the carbon layer might not be sufficient to fully mechanically support the volume expansion caused by SiMPs over lithiation and de-lithiation cycles.

Future Improvement

As a potential avenue for future exploration, the flexibility of 2D graphene sheets offers intriguing possibilities, showcasing excellent wrapping capabilities while potentially providing less mechanical support, as observed in the Pickering Emulsion project. On the other hand, SiC layers and arc-welded carbon layers exhibit robust mechanical properties but possess less elasticity. Combining these two elements could potentially result in improved coating performance, capitalizing on their respective strengths. Moreover, it is also interesting to explore a more

controlled conversion process of amorphous carbon to graphitic carbon. For example, using a catalyst (e.g. vinyl ferrocene) may lower the activation energy of graphitization transformation and decrease the temperature from 2500 °C to 625 °C; applying electrochemical transformation of amorphous carbon into highly graphitized graphite nanoflakes by using inert SnO_2 as an anode in $CaCl_2$-LiCl molten salts can achieve graphitization transformation of amorphous carbon materials at 700 °C.[28,29]

Additionally, it is intriguing to delve into the potential of silicon electrodes in various electrolyte functions and examine their relationship with battery performance. Such investigations hold promise for advancing our understanding of battery systems and optimizing their overall efficiency and functionality.

SEI as a Functional Solid-State Electrolyte

Background

The solid electrolyte interphase (SEI) is a thin interfacial layer between the alkali metal electrode and liquid electrolyte. Its formation occurs instantaneously upon contact of metal and electrolyte through both electrochemical and chemical decomposition of the solvent, and it assumes a pivotal role in enabling the reversible behavior of lithium-ion and lithium metal batteries. Back in the 1970s, researchers first found that there is a passivating layer forming on the surface of carbonaceous electrodes in lithium-ion batteries which can interfere with the deposition/dissolution process of the anode.[30] This passivating layer, defined as SEI, permits the transfer of ions while blocking the conductive pathway of electrons. Hence, it enables the reactive anode material (i.e. Li metal) to operate beyond the voltage stability window by protecting it from continuous electrochemical deposition. Since its initial discovery, increasing attention has been devoted to comprehending the SEI model and making empirical modifications to enhance battery performance. Researchers have been actively engaged in studying and modifying the SEI to improve its properties and optimize its impact on battery functionality. For example, electrolytes that promote the decomposition of anions and incorporate fluorinated components have demonstrated the ability to generate an SEI film that facilitates the reversible and uniform deposition of lithium, contributing to improved battery performanc[31]; the infiltration of electrolytes into the solid electrolyte interphase (SEI) can results in different degree of swelling, which is strongly correlated with the Coulombic efficiency (CE) of the lithium electrodeposition process.[32] With the benefit of qualitative analysis and advancements in technology, we aim to quantitatively

interpret the electrochemical properties of the solid electrolyte interphase (SEI) and directly correlate them with improvements in battery performance.

In this project, we are interested in quantifying the ionic and electronic conductivities of the solid electrolyte interphase (SEI) across different SEI chemistries and swelling states, as well as investigating how electrolyte formulations directly influence SEI properties and, consequently, battery performance. The primary challenge that remains is the development of a method for directly measuring SEI properties in various swelling states. Additionally, SEI may potentially function as a solid-state electrolyte as it is ionically conductive while electrically insulating. This is a different perspective opening another new approach within the solid-state battery literature.

Hypothesis

In this project, we introduce a simple Li|SEI||SEI|Li architecture that rapidly quantifies both ionic and electronic conductivity of SEI films formed under diverse conditions (e.g., electrolyte chemistry, swelling state). Conventional Li||Li symmetric cells would create an open circuit voltage close to zero, which introduces a challenge to distinguish the differences between a shorted cell and a symmetric cell. In our experiment, to confirm the non-shortage rate of the symmetric cells as well as to characterize the SEI ionic conductivity, we show that an OCV of ~0 V with a Nyquist plot of the electrical impedance spectrum (EIS) of Li|SEI||SEI|Li symmetric cell. It is obvious that all EIS results of non-shorted symmetric cells will exhibit two distinct semi-circles (one represents the charge transfer process occurring through the inner, denser ionic SEI layer, the other is attributed to the porous outer layer, the region between the SEI and the electrolyte),[33–35] while the EIS result of a purposely shorted cell would be flat as zero (details in EIS result section). Additionally, Li deposition and cycling performance is confirmed in a standard Li|SEI|Cu

separator free half-cell geometry. With the technique of electron microscopy and voltage profile of Li deposition, we can confirm the deposition of Li through the SEI layer on the Cu substrate.

Method and Experimental Set-up

a) SEI Formation

A conformal SEI formation requires the cleanness of a pristine Li surface. To prepare a pristine Li surface, we use a clean razor blade to scrape the surface of a 16 mm diameter metallic Li plate inside an Ar-filled glove box. Next, we stack the negative coin cell case, spacer, and the clean Li plate in respective order using 2032-coin cell pieces with the addition of 70uL of liquid electrolyte and seal it with a positive coin cell case, ensuring it is placed securely without crimping. According to various formation conditions, the optimized formation protocol requires a resting time of 48 hours inside the glove box at room temperature to complete the formation of SEI. To remove the SEI-passivated Li metal plate, the coin cell setup should be disassembled carefully without touching the SEI surface, and the Li metal should be blotted with a Kim wipe. Wet state SEI should be immediately proceeded to coin cell assembly, it has some liquid electrolyte residues (about less than 20uL) that can thicken and soften the organic and inorganic SEI structure; while dry state SEI should be allowed to rest in the glovebox for 30 minutes to permit solvent evaporation before cell assembling, it is assembled in the absent of solvent.

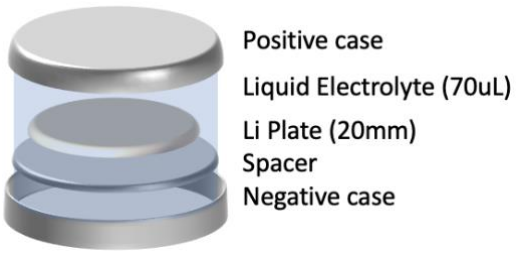

Figure 18. Schematic of SEI Formation

b) Insulating Membrane Material (O-ring)

The experimental setup of the SEI characterization test, including ionic conductivity measurement, electrical conductivity analysis, and transference number in the future, is illustrated in Figure 19. One of the most important pieces in the characterization setup is the insulating O-ring between the electrode and the positive coin cell case. It can effectively improve the success rate of tests by avoiding the shortage issues caused by the non-uniform SEI on the edge of the Li plate and further convince that all the measurements are characterizing Li-ion conducted through the middle SEI layers instead of the side membrane.

The material of the O-ring is initially selected between a Celgard separator, polyethylene membrane, Duct tape, Kapton tape, nitrile glove, and PTFE membrane based on the insulating property (both ionic and electric insulating) and chemical stability within a liquid electrolyte environment. According to our Li deposition test in standard liquid Li||Cu half-cell, only PTFE and double-layered PE membranes are ionically insulating under a current density of 0.01 mA/cm^2 (a critical current density at which o-ring membrane is insulating but SEI is ionic conductive). According to our observation, PTFE material is less stable with alkali metal and fluorinating agents. Although the stability of PTFE is verified over 3hours, we eventually chose double-layered PE as our insulating membrane to avoid any side chemical reactions. (Details see result section)

c) Ionic Conductivity measurement

According to some pioneering research on the ionic conductivity measurement, the EIS measurement is always conducted in the symmetric cell configuration since it can provide a uniform electrochemical environment with minimum effects of any stray capacitance, inductance,

or resistance in the experimental setup. [30,34–39] Also, it allows for the accurate determination of the system's response to subtle perturbations compared with standard asymmetric cells. In this project, we use symmetric Li-Li cells, in which both electrodes are pre-prepared ex-situ with SEI formed on the electrode surface as indicated in section a), are assembled in 2032-type coin cells without any separator in between electrodes. An insulating O-ring membrane is added between the electrode and positive coin cell case to prevent any shortage caused by the non-uniformity of SEI grown on the edge of Li plates. The assembled coin cell is crimped under 1000 psi to guarantee the contact between each layer. This pressure is consistently applied over all electrochemical measurements.

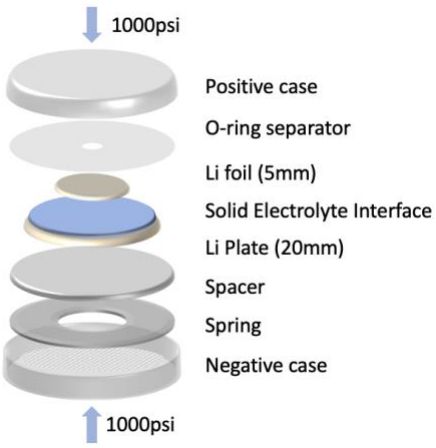

Figure 19. Symmetric Cell Geometry for SEI Characterization Test

All the EIS measurements are carried out using a Biologic VMP3 system, with a frequency range spanning from 1 MHz to 10 mHz. EC-Lab Zfit software is employed for EIS fitting, with the fitting process covering a frequency range of approximately 20 Hz to 20 kHz. Each measurement is repeated with 3 identical cells for precision and accuracy purposes.

d) Electrochemical Performance

Figure 20 illustrates a schematic of the Li||SEI||Cu half-cell assemble method developed for characterizing the electrochemical performance of SEI and qualifying the impact of SEI swelling state and chemistry on its ionic and electronic conductivity while correlating measured values with battery performance.

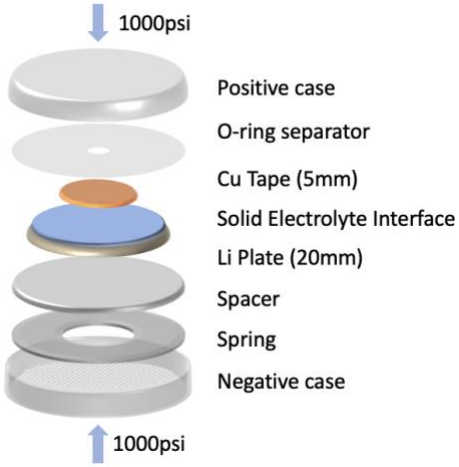

Figure 20. Li||Cu Half-Cell Geometry for Cycling Performance Test

The initial step in preparing the Li||SEI||Cu cell involves forming SEI films with different electrolyte compositions and levels of swelling. This is accomplished by immersing pristine Li foil in one of six model electrolytes for a period of 48 hours, as previously described. After this process, any excess liquid is removed either by gently blotting the SEI (resulting in a swollen state) or by drying it for 30 minutes in a glovebox (resulting in a dry state). We then assemble type 2032-coin cells by placing Cu directly in contact with the SEI-coated Li metal, without the use of a separator. Despite being crimped at 1,000 psi pressure, the Li||SEI||Cu cell does not short circuit and exhibits an open circuit voltage of approximately 1.8 V~2.2V, which is typical of traditional Li-Cu half cells. To evaluate the SEI's ionic and electrical conductivity as a function of its chemical composition and degree of swelling, we use standard methods in the solid-state electrolyte

literature, including AC impedance and DC polarization, as outlined in the previous methods section.

Result and Discussion

a) SEI formation Result

Initially, the uniformity of SEI formation is confirmed with Scanning Electron Microscopy. The example top SEM images of SEI formed by soaking Li plate in 1 M $LiPF_6$ in EC/DEC (50:50) and 4 M LiFSI in DME are shown in Figure 21. It is clear that there are no significant cracks or holes on the top surface of SEI, which again proves the reliability and repeatability of our formation method.

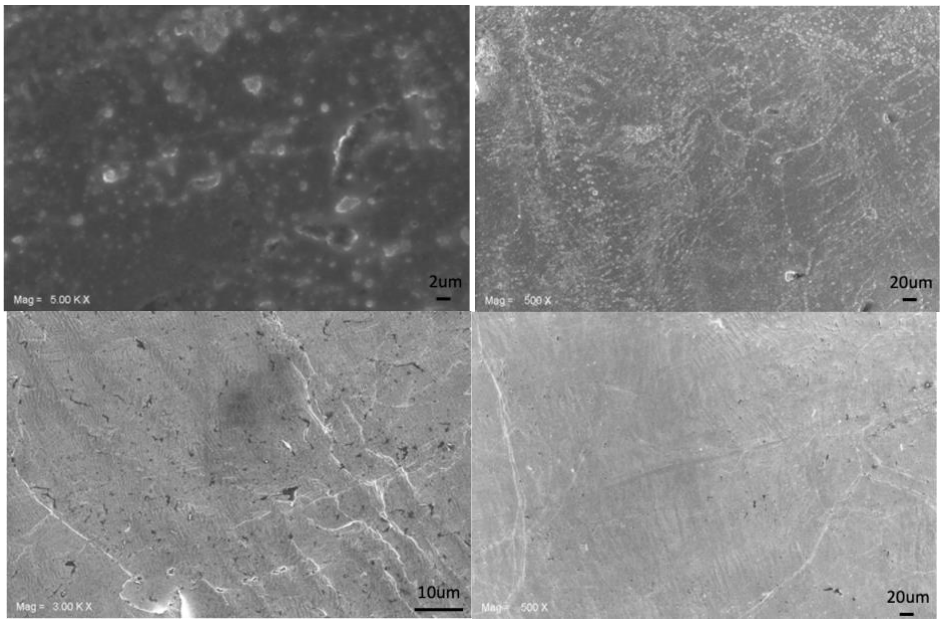

Figure 21. Top SEM Image of SEI Formation on Li Plate: 1 M $LiPF_6$ in EC/DEC (top); 4 M LiFSI in DME (bottom)

Then, the cross-sectional SEM image of SEI layer on the Li plate further confirms the uniformity of thickness of this passivation layer. Although all the cross-sectional SEM was taken at the drying state after rinsing with the appropriate solvent and pressing under the same pressure (crimped with

a biologic clamp), the thickness of SEI varies with different concentration of electrolytes and different chemical compositions of salt. In Figure 22, we provide a statistical analysis of the thickness of each SEI (solid electrolyte interphase) by examining over 30 random points in each electrolyte. The data was analyzed using a histogram, allowing us to determine the average thickness of the SEI.

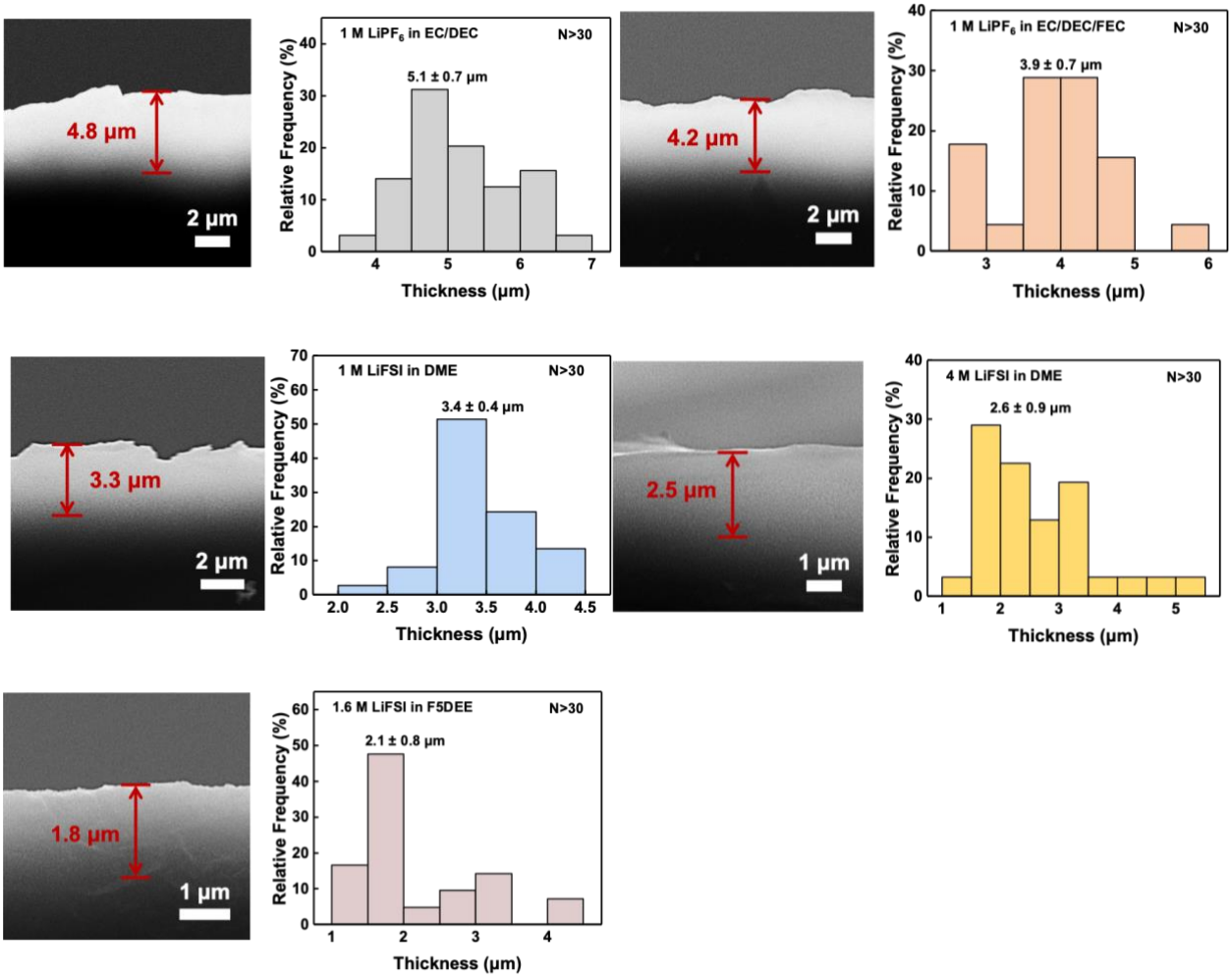

Figure 22. Cross Sectional SEM of SEI and Statistical Result of SEI Thickness

b) Insulating O-ring Membrane Selection

As mentioned earlier, the insulating membrane plays a crucial role in our setup by addressing the short-circuit concerns arising from the non-uniformity of the solid electrolyte interphase (SEI) at

the edge of the lithium plate. Also, it can restrict the conduction pathways of lithium solely through the SEI layer and improve the accuracy of our characterization measurements.

During the selection process of the insulating material, which should possess both ionic and electrical insulation properties, we conduct tests using various membrane materials in a Li|membrane|Cu liquid half-cell configuration. This configuration includes a 20 μL liquid electrolyte (1 M $LiPF_6$ in EC/DEC), creating a "flooded" environment. Since in the geometry of our swollen state SEI measurement, the maximum amount of electrolyte residue remaining is less than 20 μL after blotting with a Kim wipe, if the material is insulating under this "flooded" condition, it satisfies our requirements in all the characterization measurements.

Here, the voltage profile of Li deposition through each membrane is presented. According to the voltage profile, Kapton tape, single and double tape, nitrile glove, and double duct tape has stable Li deposition over 30 hours at the small current density. However, PTFE has a voltage profile stabilized at 1.1 V and double PE has a clear open circuit (voltage drops below -20 V) within a few seconds. According to our research and observation, the PTFE material is less stable with alkali metal and fluorinating agents. Hence, we used a double PE membrane as our optimized insulating membrane.

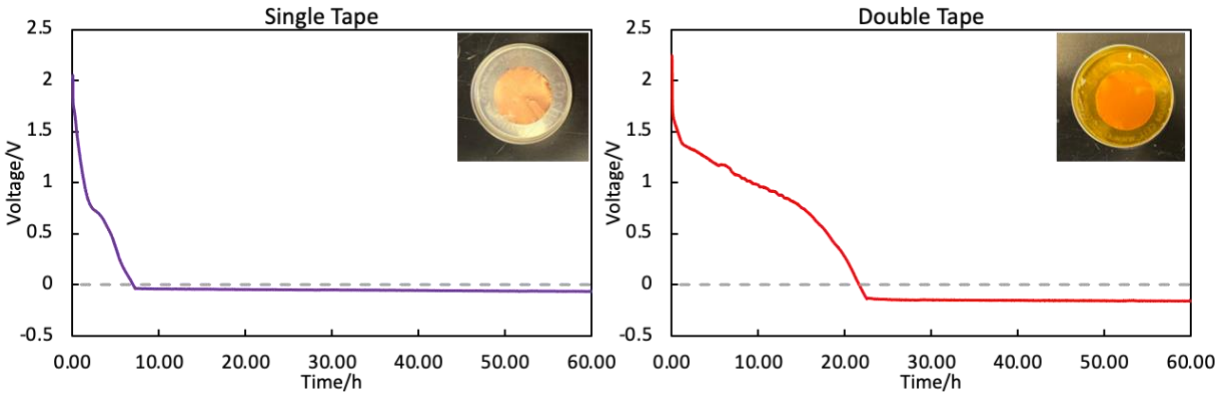

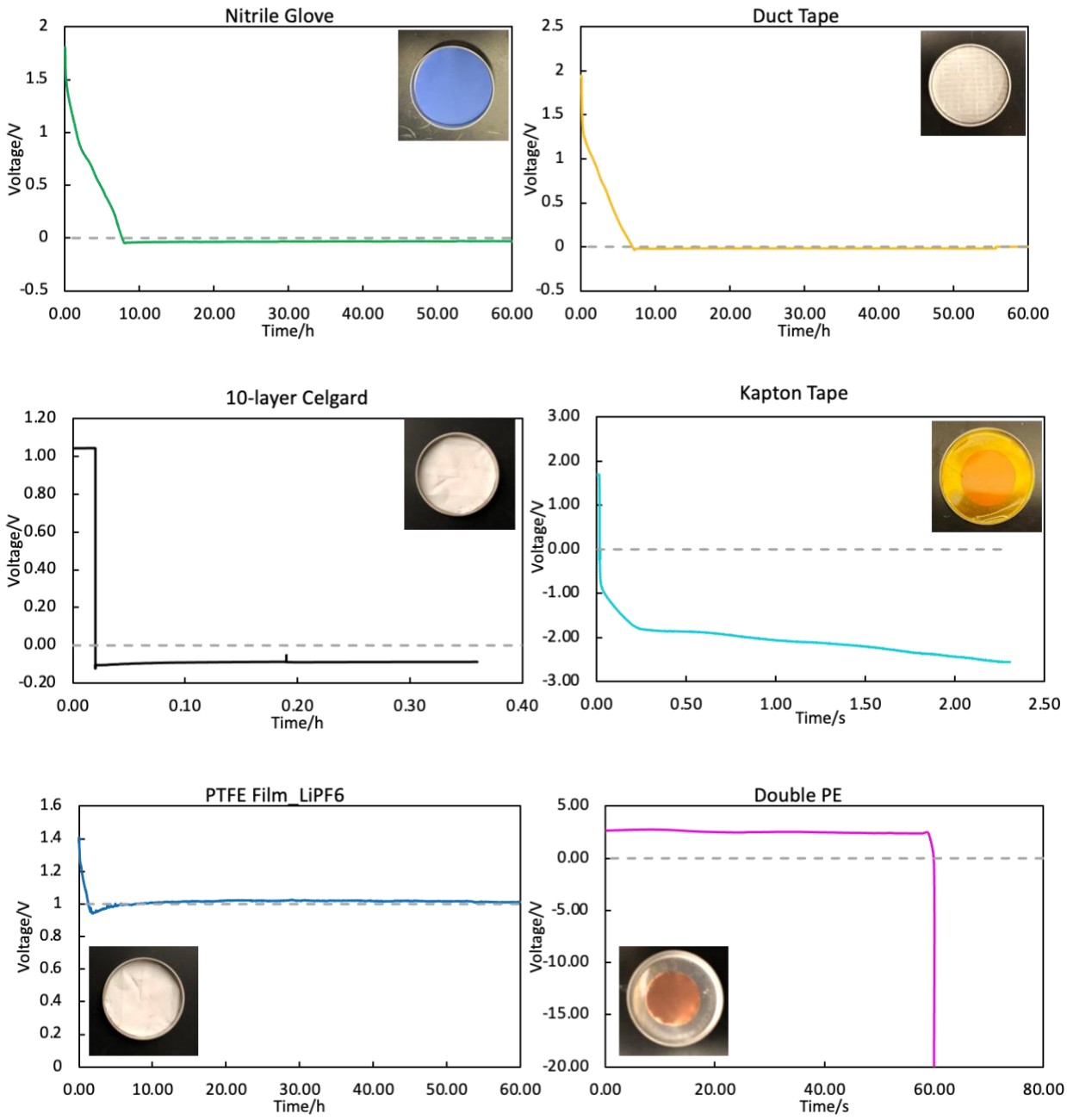

Figure 23. Li Deposition Voltage Profile through Different Membrane

c) Ionic conductivity Measurement

According to our Nyquist plot of the electrical impedance spectrum of Li||SEI||Li symmetric cell, all results exhibit two distinct semi-circles. This phenomenon is also observed in previous Li symmetric cell SEI measurements as shown by Gallant et al.[35] According to the pioneering

literature, the high-frequency range (100 kHz-20 Hz) of the impedance spectrum is associated with the charge transfer process occurring through the inner, denser ionic SEI layer. On the other hand, the low-frequency range (10 Hz to 10 mHz) of the impedance spectrum is attributed to the porous outer layer, which represents the interphase region between the SEI and the electrolyte.[34,40] Additionally, this outer range may also be attributed to the minor reaction between the electrolyte and SEI layer during the soaking process. It may also explain why the swollen state has a more obvious second semi-circle than the dry state.

Here, we used an EC-Lab Zfit software to fit the model with an equivalent circuit. The equivalent circuit detail is referring to Gallant's previous publication (as our set-up is very similar to their symmetric cell geometry). The result (we have obtained so far) of the total ionic resistance of SEI is summarized in the Figure below for both swollen and dry state SEI. Here, we initially test two different electrolytes in our optimized set-up, 1 M $LiPF_6$ in EC/DEC and 4 M LiFSI in DME. In the future, when the thickness and area of each SEI configuration are finalized and when we obtained more consistent reliable EIS data, the actual value of ionic conductivity will be normalized with the thickness and area/size of SEI through the equation and the data of other SEI made from different electrolytes formulation will be collected soon.

$$\sigma_i = \frac{L}{R_{sei,i}\, A}$$

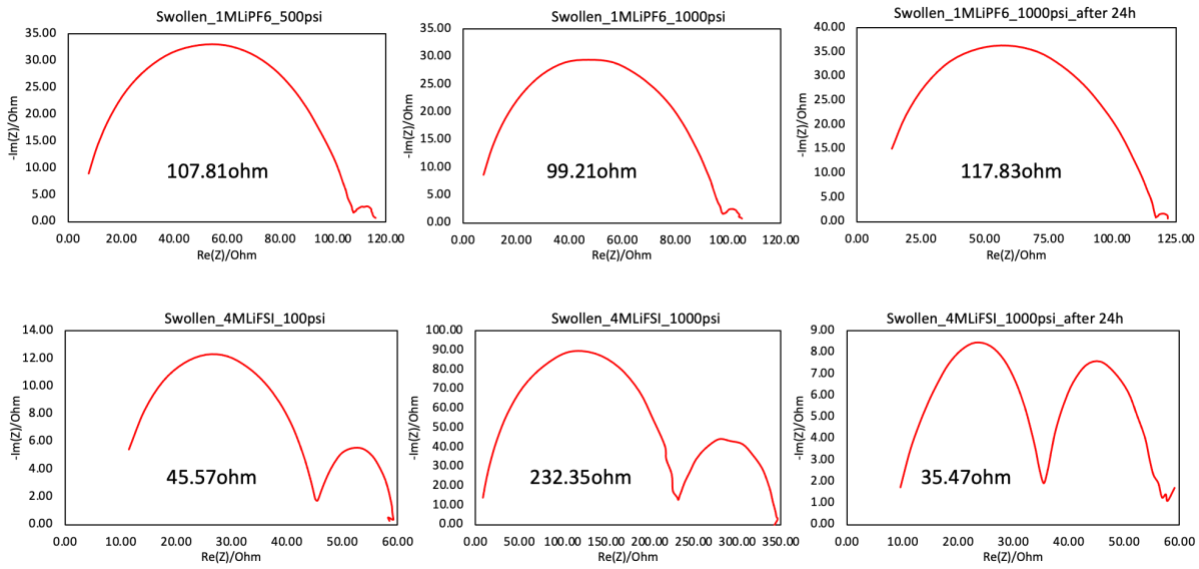

Figure 24. Ionic Conductivity of Swollen State SEI at varying pressure condition

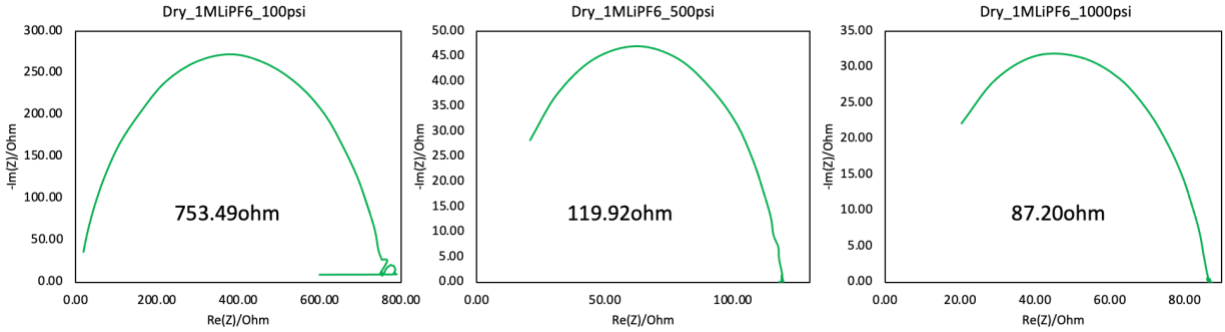

Figure 25. Ionic Conductivity of Dry State SEI at varying pressure condition

d) Electrochemical Performance (Li deposition and cycling performance)

The electrochemical cycling performance is conducted in a Li|SEI|Cu half-cell configuration without any traditional separator. Conventional wisdom would suggest that the coin cell must short without any separator between Cu and Li, however, our coin cell geometry can withstand 1000 psi pressure without shorting. This again proves the robust property of the SEI layer on the surface of the Li metal plate. Also, it was noticed that Li ions can deposit through the SEI layer and form Li

nuclei on the Cu substrate in the SEM image. With this evidence, we further cycle the coin cell at 0.01 mA/cm^2. The electrochemical data shows an open circuit voltage of 1.66 V and an initial Coulombic efficiency of 57.0%. This cycling performance can be stabilized for at least 5 cycles under room temperature with swollen state SEI made of 1 M $LiPF_6$ in EC/DEC. In the future, we will test other SEI and collect more data for the interpretation of the relationship between electrolyte chemistry and cycling capability.

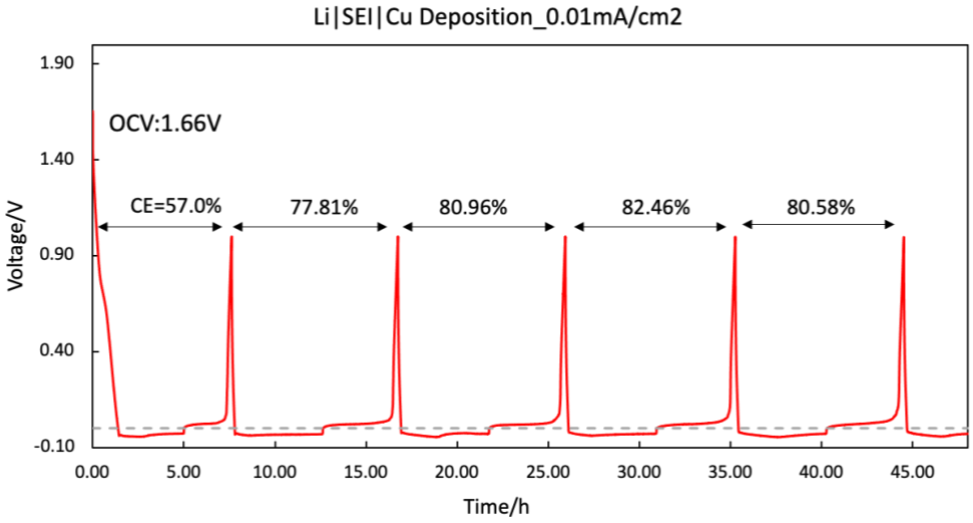

Figure 26. Cycling Performance of SEI at Swollen State

Future Plan

First, the ionic conductivity measurement is incomplete at this moment since we focused on defining the synthesis method, optimizing the experimental set-up and test conditions, and interpreting the reliability and repeatability of our test results over the past quarter. Now we are ready to collect more data of various types of SEI soaked in different electrolyte formulations.

In the future, we will analyze the relationship between the swelling state of SEI and its electrochemical properties (such as the ratio between ionic and electrical conductivity) in a broad range of electrolyte chemistry.

Second, the method of electronic conductivity measurement is not yet verified

Electronic Conductivity Measurement

The experimental set-up of electronic conductivity measurement of some conventional solid-state electrolytes (i.e. LLZO and Li3PS4) is to use symmetric cell geometry with ion-blocking/inert electrode material (such as Cu) under the DC polarization process.[41] Since these electrolytes are not thermal dynamically stable with Li metal, subtle decomposition of electrolytes can influence the value of conductivity measurement noticeably.[42] In this experiment, a small voltage (i.e. 100mV) is initially applied over the symmetric cell to create ion migration. Over time, the concentration of lithium ions builds up at the negative electrode side, creating a concentration gradient. At a steady state, the diffusion of lithium ions toward the positive electrode will counteract the polarization that we apply so that there will be no lithium-ion flux within the electrolyte. Therefore, at a steady state, the measured current is considered only from electronic carriers, and the electronic conductivity can then be determined from this current (steady-state current).

Another traditional method for electronic conductivity measurement is named as Hebb-Wagner method.[41,43,44] It can only be applied to those electrolytes who have stability against Li metals. For example, this method has been applied in Rettie's work[44] to estimate the electronic conductivity in a Hebb-Wagner Cell. They used a Li metal electrode (reversible for both ions and electrons) and an ion blocking electrode to estimate the electronic conductivity of LiPON, polymer-based

electrolytes, etc. However, it is noticed that the two-electrode set-up will include additional contact resistance and underestimate the real electronic conductivity.

For the expected result, it will present a current vs. time diagram in which the current first decreases over a constant applied voltage then reaches steady state. The calculation of the electronic conductivity can use the equation below, where L is the thickness of SEI, A is the surface area of SEI, $R_{SEI,e}$ is the total electronic resistance of SEI calculated from $V_{applied}/I_{ss}$.

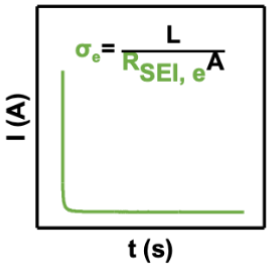

Figure 27. Expected Electronic Conductivity Measurement of SEI

The main challenges remaining in our project are the limitation of the choice of electrodes and the effect of the contact resistance between each layer. Since we need to quantify the conductivity of SEI formed on the Li metal surface, it is impossible to use ionic insulating/inert symmetric electrodes. Hence, we first propose to test with asymmetric cell geometry, similar to Figure *20,* using Hebb-Wagner's method and decide if any modification is needed based on the preliminary result.

Third, it is also interesting to quantify the transference number of SEI layer and analyze the relationship between transference number and electrochemical performance. Here, a brief introduction and method proposal of transference number measurement is presented as well as some raw data sets.

Transference Number measurement

To further investigate the process of ionic transportation through the solid electrolyte interface and explore the limitation of the charging/discharging rate of the solid-state battery, the transference number is measured to quantify the mobility of ions (i.e. Li^+ and PF_6^-) within the solid electrolyte interface. Specifically, the magnitude of the transference number quantifies how much current is carried by the lithium ions versus the total current conducted in the battery. According to the definition, the summation of the current fraction carried by cations (t_+) and the fraction carried by anions (t_-) equals 1.

$$t_+ = \frac{D_+}{D_+ + D_-} \; ; t_- = \frac{D_-}{D_- + D_+}$$

where D is the diffusion coefficient of ions.

In the majority of liquid electrolytes (such as LiPF6 in EC/DEC and LiFSI in DME), the partial current carried by cations is smaller than the current carried by anions due to the solvation structure surrounding Li^+; the transference number of 1 M $LiPF_6$ in EC/DEC Li||Cu half-cell is about 0.3. According to some pioneer electrolyte research, the magnitude of transference number can significantly affect the limitation of lithiation and de-lithiation rate. For instance, a larger transference number means more current is conducted through Li^+ transportation; therefore, the consumption of Li on the positive electrode surface (the production on the negative electrode) can be replenished by the electric migration efficiently, leading to a smaller concentration gradient in the electrolyte environment. As a result, the mitigation of the concentration gradient can reduce the resistance ionic resistance on the electrode surface. Hence, a larger transference number is favored in reversible LIBs to sustain an indefinite electrolyte environment under diverse charging and discharging protocols.

Methodology

The measurement of the transference number in this project is inspired by the Bruce-Vincent Method published in 1987.[45,46] In the Bruce-Vincent Method, it is assumed that first, the ions are fully dissociated in the electrolyte; second, the behavior of ions obeys Nernst Einstein equation. The measurement of the transference number is conducted through Lithium symmetric cells (Figure 19). In the beginning, a small polarization potential (5mV) is applied to generate a small concentration gradient. The initial current (I_o) takes into account both cations and anions movement in the electrolyte system. Over time, the migration of anions towards the positive side and the diffusion of anions towards the negative side balance off at a steady state. Hence, the steady state current (I_{ss}) is only conducted through the migration and diffusion of Li^+. Here, the first version of the transference number is calculated using the following equation

$$t_+ = \frac{Iss}{Io}$$

Later, to improve the accuracy of measurement, the second version of the equation includes the interfacial resistance from the coin cell set-up and electrical contact between each layer. Since the resistance may change over time, two EIS measurements are conducted to measure the ionic resistance before and after the transference number test.

$$t_+ = \frac{Iss(\Delta V - I_o R_{p,o})}{Io(\Delta V - I_{ss} R_{p,ss})}$$

The equation is derived from Bruce-Vincent's Method. ΔV is the applied potential (5mV) over the measurement, $R_{p,o}$ and $R_{p,ss}$ are the interfacial resistances at the initial and steady state condition. The value of R_p is measured using the same methodology described in the EIS measurement section.

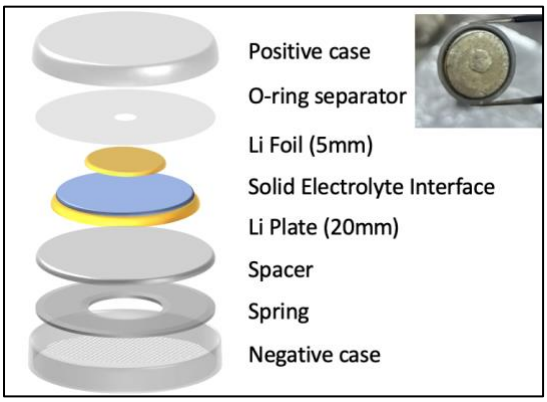

Figure 28. Schematic of Transference Number Measurement

During the experiment, it is important to resolve the problem of inconsistency in contact since both EIS measurement and DC polarization are sensitive to the fluctuation of electrical contact. Several strategies have been applied to tackle the challenges: first, we pre-baked the coin cell at 60C over 24h after the cell assemble to stabilize the SEI layer and the contact between each layer; second, we crimped the coin cell at 0 psi, 100 psi, 500 psi, and 1000 psi to avoid the void space between layers; moreover, we tried to use silver epoxy, a conductive glue-like material to minimize the void space. Eventually, the optimized set-up is a combination of 3 h rest at room temperature, 1000 psi, and 30 min rest between each measurement since higher pressure can cause shortage more easily and non-uniform silver epoxy can introduce unnecessary impedance factors.

Preliminary Result

Here, we did some preliminary tests on the transference number measurement of 1 M $LiPF_6$ in EC/DEC and 4 M LiFSI in DME SEIs under both swollen and dry states. It is noticed that all the cells have initial and final EIS measurements, which proves the symmetric cell does not short during the measurements. Without normalizing with impedance and applied voltage, the estimated transference number is close to 1 for both electrolytes at dry state. Although the result values are

not always consistent yet, it is clear that the electrical impedance changes before and after the measurement. This may be due to the changing interfacial resistance from the coin cell set-up and electrical contact between each layer as mentioned previously. In the future, we need to conduct more experiments to confirm the reliability and repeatability of this result. Once the result is consistent, other types of SEI can also be quantified with this method.

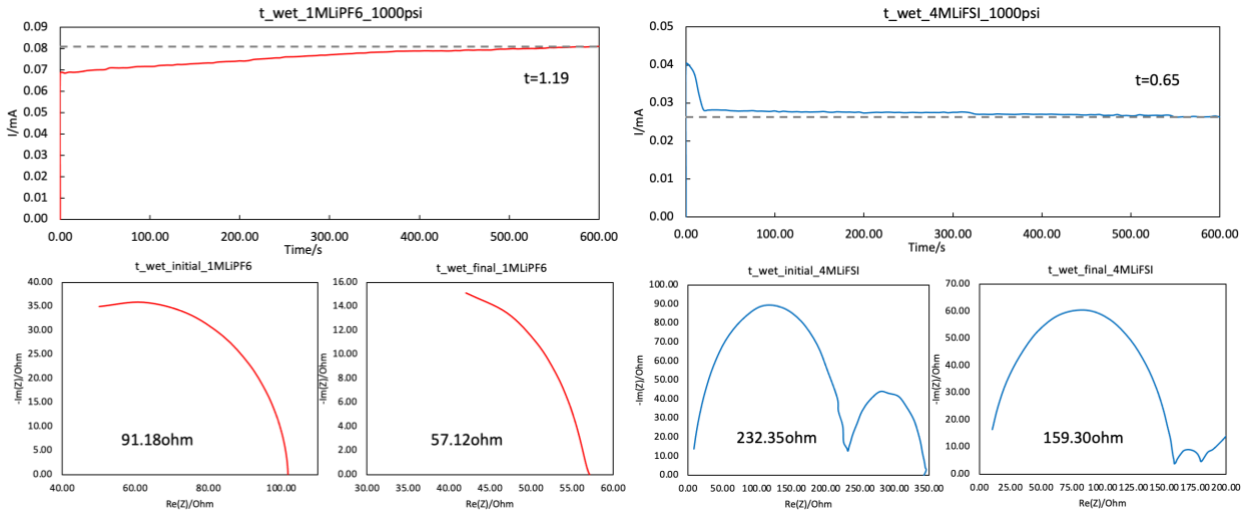

Figure 29. Preliminary Result of Transference Number at Swollen State

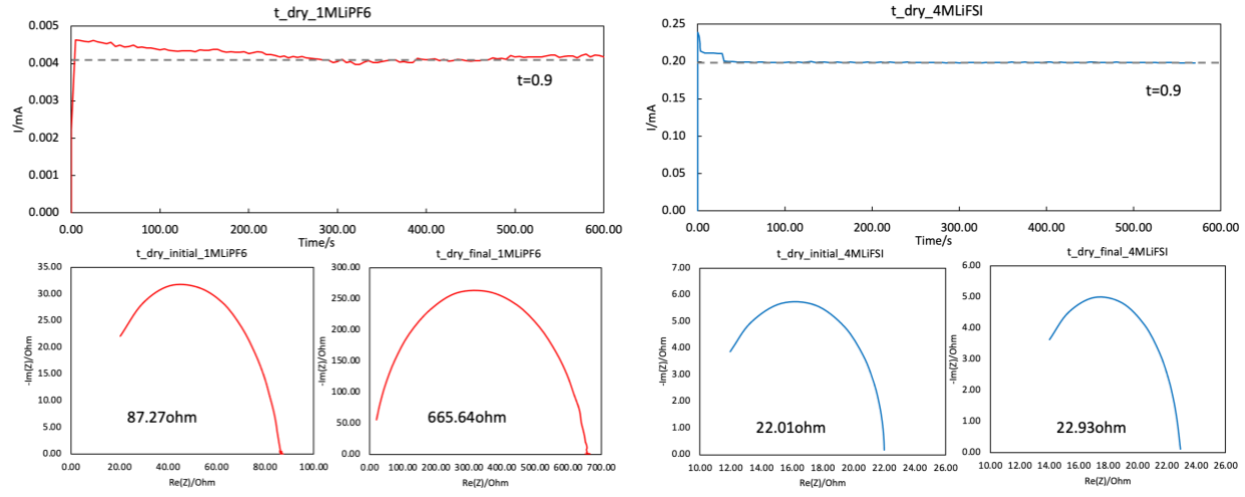

Figure 30. Preliminary Result of Transference Number at Dry State

Conclusion

This work aims to contribute to the advancement of engineered electrode materials and enhance our understanding of the solid electrolyte interphase (SEI), ultimately driving innovation in the field of high-performance batteries. Given the time constraints, the reported method and preliminary results presented in this study are current based on our existing knowledge. However, further research is essential to comprehensively address the broader scope of work.

In response to the growing demand for energy storage technology, battery research has expanded its scope beyond lithium-ion batteries (LIBs) to include zinc and sodium-ion batteries.[47,48] Within the realm of LIBs, while graphite anodes and transition metal cathodes have gained widespread usage due to their stability and reasonable energy capacity, they still possess limitations in terms of small volumetric capacity, limited environmental friendliness, mining-related health risks, and safety concerns and require relentless effort on creative innovations.[6,49,50] On the material level, exploration is encompassing not only silicon anodes but also $LiFePO_4$, vanadium cathodes, and other alternatives.[51,52] On the technology level, advancements in technologies like cryo-electron microscopy (cryo-EM) are opening up new avenues for broader comprehension and exploration in battery research.[32,53] The solid electrolyte interphase (SEI) is just one component within this extensive field, as there are other aspects such as lithium/sodium dendrite formation and various microscopic phenomena that await detailed exploration and investigation.

Moreover, the collaboration between academia and industry necessitates the investigation of strategies for streamlined material synthesis and efficient structural engineering. In a broader context, research should not be confined to the boundaries of laboratories and academic institutions alone; it should strive to make significant contributions on a larger scale toward the development of a sustainable world.

Reference

1. CO2 Emissions in 2022 – Analysis - IEA. https://www.iea.org/reports/co2-emissions-in-2022.
2. Lithium-ion battery demand forecast for 2030 | McKinsey. https://www.mckinsey.com/industries/automotive-and-assembly/our-insights/battery-2030-resilient-sustainable-and-circular.
3. Lithium-ion battery demand forecast for 2030 | McKinsey. https://www.mckinsey.com/industries/automotive-and-assembly/our-insights/battery-2030-resilient-sustainable-and-circular.
4. Electrifying insights: How automakers can drive electrified vehicle sales and profitability | McKinsey. https://www.mckinsey.com/industries/automotive-and-assembly/our-insights/electrifying-insights-how-automakers-can-drive-electrified-vehicle-sales-and-profitability.
5. Wang, Z. *et al.* Overcharge-to-thermal-runaway behavior and safety assessment of commercial lithium-ion cells with different cathode materials: A comparison study. *Journal of Energy Chemistry* **55**, 484–498 (2021).
6. Zhang, H., Yang, Y., Ren, D., Wang, L. & He, X. Graphite as anode materials: Fundamental mechanism, recent progress and advances. *Energy Storage Mater* **36**, 147–170 (2021).
7. Ozanam, F. & Rosso, M. Silicon as anode material for Li-ion batteries. *Materials Science and Engineering: B* **213**, 2–11 (2016).
8. Mauger, A. *et al.* Composite anodes for lithium-ion batteries: status and trends. *AIMS Materials Science 2016 3:1054* **3**, 1054–1106 (2016).

9. Andersen, H. F. *et al.* Silicon-Carbon composite anodes from industrial battery grade silicon. *Scientific Reports 2019 9:1* **9**, 1–9 (2019).

10. Zhai, W. *et al.* Walnut-inspired microsized porous silicon/graphene core–shell composites for high-performance lithium-ion battery anodes. *Nano Research 2017 10:12* **10**, 4274–4283 (2017).

11. Wang, J. & Cui, Y. Electrolytes for microsized silicon. *Nature Energy 2020 5:5* **5**, 361–362 (2020).

12. Chan, C. High-performance lithium battery anodes using silicon nanowires. *Nat. Nanotechnol.* **3**, 31–35 (2008).

13. Choi, S., Kwon, T.-W., Coskun, A. & Choi, J. W. *Highly elastic binders integrating polyrotaxanes for silicon microparticle anodes in lithium ion batteries*. https://www.science.org.

14. Li, Y. *et al.* Growth of conformal graphene cages on micrometre-sized silicon particles as stable battery anodes. *Nature Energy 2016 1:2* **1**, 1–9 (2016).

15. Lu, Z. *et al.* Nonfilling carbon coating of porous silicon micrometer-sized particles for high-performance lithium battery anodes. *ACS Nano* **9**, 2540–2547 (2015).

16. Wu, H. & Cui, Y. Designing nanostructured Si anodes for high energy lithium ion batteries. *Nano Today* **7**, 414–429 (2012).

17. Park, K.-Y. *et al.* Concurrently Approaching Volumetric and Specific Capacity Limits of Lithium Battery Cathodes via Conformal Pickering Emulsion Graphene Coatings. *Adv Energy Mater* **10**, 2001216 (2020).

18. Rodier, B., de Leon, A., Hemmingsen, C. & Pentzer, E. Controlling Oil-in-Oil Pickering-Type Emulsions Using 2D Materials as Surfactant. (2017) doi:10.1021/acsmacrolett.7b00648.

19. Ferchichi, K., Hbaieb, S., Amdouni, N., Pralong, V. & Chevalier, Y. Pickering emulsion polymerization of polyaniline/LiCoO2 nanoparticles used as cathode materials for lithium batteries. *Ionics (Kiel)* **20**, 1301–1314 (2014).

20. Morita, M., Ohmi, T., Hasegawa, E., Kawakami, M. & Ohwada, M. Growth of native oxide on a silicon surface. *J Appl Phys* **68**, 1272–1281 (1990).

21. Wu, J. *et al.* Poly-dopamine coated graphite oxide/silicon composite as anode of lithium ion batteries. *Powder Technol* **311**, 200–205 (2017).

22. El-Kady, M. F., Strong, V., Dubin, S. & Kaner, R. B. Laser scribing of high-performance and flexible graphene-based electrochemical capacitors. *Science (1979)* **335**, 1326–1330 (2012).

23. What is Arc Welding? - Definition and Process Types - TWI. https://www.twi-global.com/technical-knowledge/faqs/what-is-arc-welding.

24. Yu, C. *et al.* Silicon Carbide as a Protective Layer to Stabilize Si-Based Anodes by Inhibiting Chemical Reactions. *Nano Lett* **19**, 5124–5132 (2019).

25. Chung, C. K. & Wu, B. H. Reaction of carbon and silicon at high temperature deposition. *3rd IEEE International Conference on Nano/Micro Engineered and Molecular Systems, NEMS* 136–139 (2008) doi:10.1109/NEMS.2008.4484304.

26. Schuepfer, D. B. *et al.* Assessing the structural properties of graphitic and non-graphitic carbons by Raman spectroscopy. *Carbon N Y* **161**, 359–372 (2020).

27. Yu, C. *et al.* Silicon Carbide as a Protective Layer to Stabilize Si-Based Anodes by Inhibiting Chemical Reactions. *Nano Lett* **19**, 5124–5132 (2019).

28. Tu, J. *et al.* High-efficiency transformation of amorphous carbon into graphite nanoflakes for stable aluminum-ion battery cathodes. *Nanoscale* **11**, 12537–12546 (2019).

29. Nakamizo, M., Kammereck, R. & Walker, P. L. Laser raman studies on carbons. *Carbon N Y* **12**, 259–267 (1974).

30. Peled, E. & Yamin, H. Solid Electrolyte Interphase (SEI) Electrodes. Part 1. The Kinetics of Lithium in LiAlCl4-SOCl2. *Isr J Chem* **18**, 131–135 (1979).

31. Chen, J. *et al.* Electrolyte design for LiF-rich solid–electrolyte interfaces to enable high-performance microsized alloy anodes for batteries. *Nature Energy 2020 5:5* **5**, 386–397 (2020).

32. Zhang, Z. *et al.* Capturing the swelling of solid-electrolyte interphase in lithium metal batteries. *Science (1979)* **375**, 66–70 (2022).

33. Vadhva, P. *et al.* Electrochemical Impedance Spectroscopy for All-Solid-State Batteries: Theory, Methods and Future Outlook. *ChemElectroChem* **8**, 1930–1947 (2021).

34. Hodge, I. M., Ingram, M. D. & West, A. R. Impedance and modulus spectroscopy of polycrystalline solid electrolytes. *J Electroanal Chem Interfacial Electrochem* **74**, 125–143 (1976).

35. Guo, R. & Gallant, B. M. Li2O Solid Electrolyte Interphase: Probing Transport Properties at the Chemical Potential of Lithium. *Chemistry of Materials* **32**, 5525–5533 (2020).

36. E., P. The Electrochemical Behavior of Alkali and Alkaline Earth Metals in Nonaqueous Battery Systems—The Solid Electrolyte Interphase Model. *J. Electrochem. Soc.* **126**, 2047 (1979).

37. Peled, E. & Menkin, S. Review—SEI: Past, Present and Future. *J Electrochem Soc* **164**, A1703–A1719 (2017).

38. Yan, Z. Symmetric Cells as an Analytical Tool for Battery Research: Assembly, Operation, and Data Analysis Strategies. *J Electrochem Soc* **170**, 020521 (2023).

39. Petibon, R. *et al.* Study of Electrolyte Additives Using Electrochemical Impedance Spectroscopy on Symmetric Cells. *J Electrochem Soc* **160**, A117–A124 (2013).

40. Guo, R. & Gallant, B. M. Li2O Solid Electrolyte Interphase: Probing Transport Properties at the Chemical Potential of Lithium. *Chemistry of Materials* **32**, 5525–5533 (2020).

41. Han, F. *et al.* High electronic conductivity as the origin of lithium dendrite formation within solid electrolytes. *Nature Energy 2019 4:3* **4**, 187–196 (2019).

42. Shin, B. R. *et al.* Comparative Study of TiS2/Li-In All-Solid-State Lithium Batteries Using Glass-Ceramic Li3PS4 and Li10GeP2S12 Solid Electrolytes. *Electrochim Acta* **146**, 395–402 (2014).

43. Hebb, M. H. Electrical Conductivity of Silver Sulfide. *J Chem Phys* **20**, 185–190 (1952).

44. Vadhva, P. *et al.* Electrochemical Impedance Spectroscopy for All-Solid-State Batteries: Theory, Methods and Future Outlook. *ChemElectroChem* **8**, 1930–1947 (2021).

45. Transport and transference in battery electrolytes · Matt Lacey. http://lacey.se/science/transference/.

46. Evans, J., Vincent, C. A. & Bruce, P. G. Electrochemical measurement of transference numbers in polymer electrolytes. *Polymer (Guildf)* **28**, 2324–2328 (1987).

47. Song, M., Tan, H., Chao, D. & Fan, H. J. Recent Advances in Zn-Ion Batteries. *Adv Funct Mater* **28**, 1802564 (2018).

48. Yabuuchi, N., Kubota, K., Dahbi, M. & Komaba, S. Research development on sodium-ion batteries. *Chem Rev* **114**, 11636–11682 (2014).

49. Daniel, C., Mohanty, D., Li, J. & Wood, D. L. Cathode materials review. *AIP Conf Proc* **1597**, 26–43 (2014).

50. Xia, Y., Zheng, J., Wang, C. & Gu, M. Designing principle for Ni-rich cathode materials with high energy density for practical applications. *Nano Energy* **49**, 434–452 (2018).

51. Ahsan, Z. *et al.* Recent progress in capacity enhancement of LiFePO4cathode for Li-Ion batteries. *Journal of Electrochemical Energy Conversion and Storage* **18**, 10801–10802 (2021).

52. Tang, H. *et al.* Vanadium-Based Cathode Materials for Rechargeable Multivalent Batteries: Challenges and Opportunities. *Electrochemical Energy Reviews 2018 1:2* **1**, 169–199 (2018).

53. Cheng, Y. Single-particle cryo-EM-How did it get here and where will it go. *Science (1979)* **361**, 876–880 (2018).